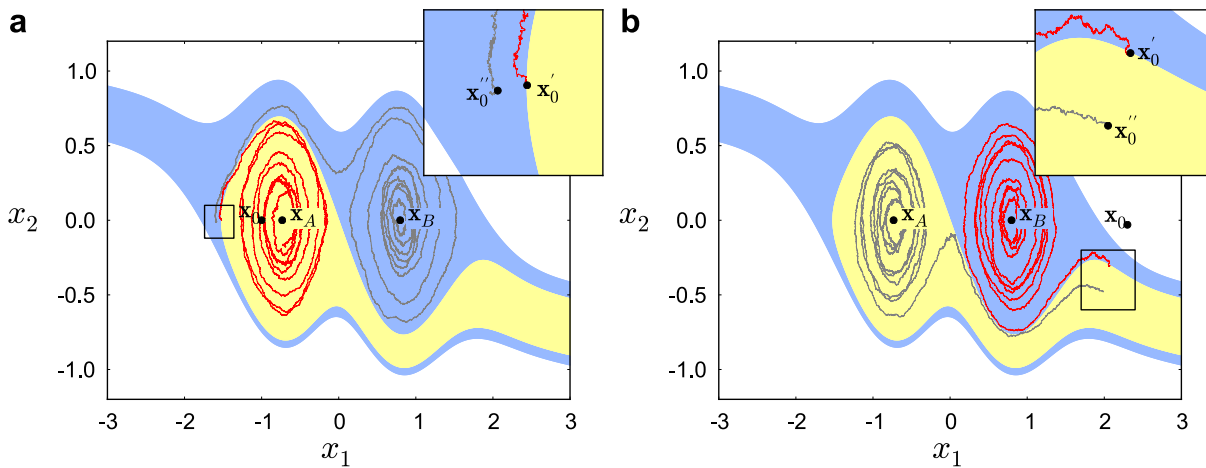


Realistic Control of Network Dynamics
S.P. Cornelius, W.L. Kath, and A.E. Motter
Supplementary Information

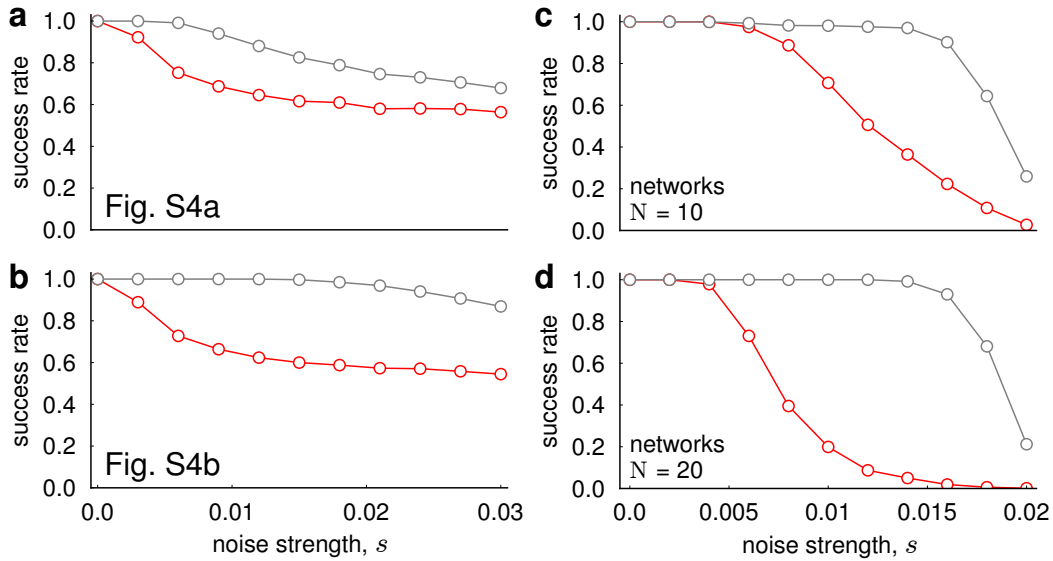
Contents

Supplementary Figures	2
Supplementary Figure S1	2
Supplementary Figure S2	3
Supplementary Figure S3	4
Supplementary Figure S4	5
Supplementary Figure S5	6
Supplementary Figure S6	7
Supplementary Figure S7	8
Supplementary Figure S8	9
Supplementary Table	10
Supplementary Table S1	10
Supplementary Methods	11
Termination criteria and control parameters	11
Construction of random genetic networks	11
Drawbacks of alternative implementations	11
Supplementary Discussion	13
Illustration of control procedure in two dimensions	13
Effectiveness of control in the presence of fractal basins	13
Effectiveness of control in the presence of riddled basins	14
Effectiveness and computational efficiency	15
Comparison with existing literature	17
Effects of stochasticity	18
Effects of parameter uncertainty	20

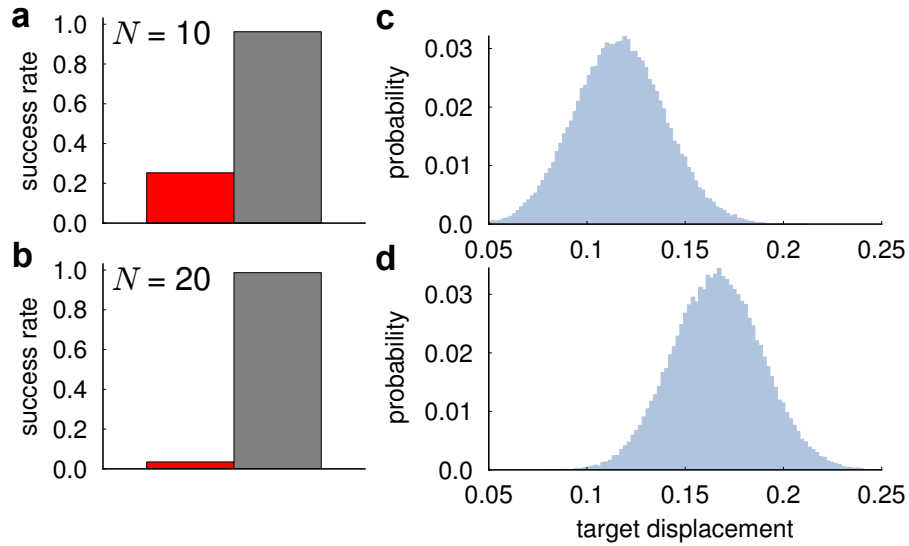
Supplementary Figures



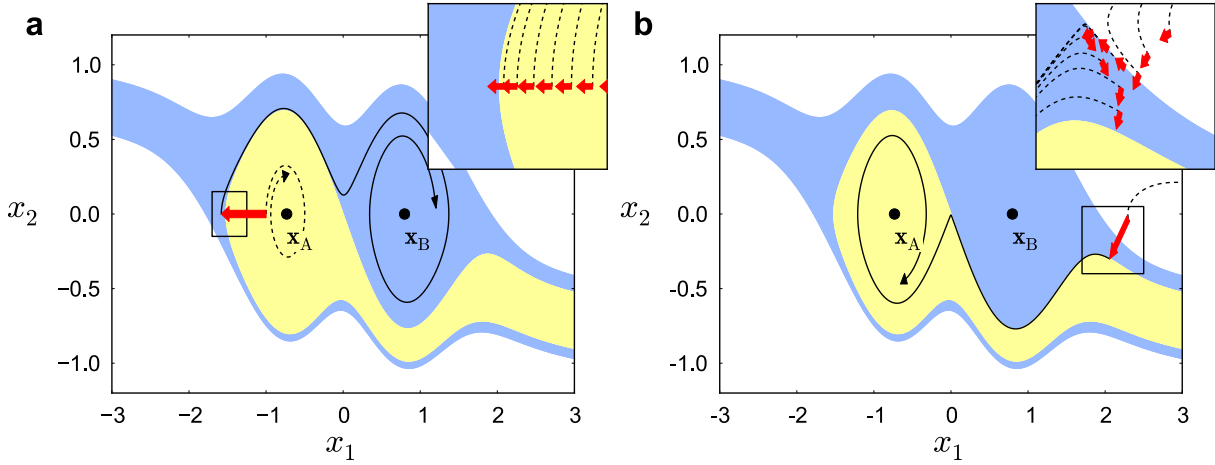
Supplementary Figure S1: Effects of stochasticity. Scenarios (a) and (b) correspond to the control problems depicted in Supplementary Figures S4a and S4b, respectively, where x_A and x_B are the attractors of the noiseless dynamics and yellow and blue their corresponding basins of attraction in the deterministic case. The intervention $x_0 \rightarrow x'_0$ represents the compensatory perturbation which, in the absence of noise, results in an orbit that carries the system to the target (x_B and x_A , respectively). This example illustrates that when noise is added to the dynamics, however, the system may fail to reach the target attractor, possibly approaching the other attractor instead (red curves). This can be attributed to the proximity of x'_0 to the corresponding basin boundary. The situation can be remedied by making an additional perturbation $x'_0 \rightarrow x''_0$ that places the system further inside the target basin of attraction, increasing the likelihood that the noisy orbit (grey) will reach the target. The noise strength is $s = 0.03$ for all orbits pictured here.



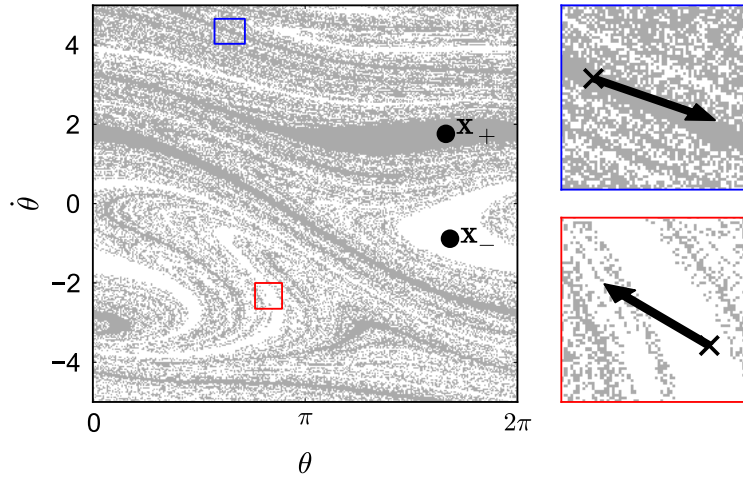
Supplementary Figure S2: Robustness of compensatory perturbations against noise. The curves indicate the success rate of compensatory perturbations predicted using deterministic models when noise of r.m.s. amplitude s is added to the dynamics, for the compensatory perturbations as predicted using our original computational approach (red), and modified compensatory perturbations that are systematically identified to be further inside the target basin of attraction (grey). **(a, b)** Mechanical example system, with the initial target states considered in Supplementary Figures S4a and S4b, respectively. **(c, d)** Ensemble of 100 random networks and initial and target states as considered in Supplementary Figure S7 for sizes $N = 10$ and 20 , respectively. In all scenarios, a point corresponds to 1,000 independent sample paths of the noisy dynamics. Each point in **(a, b)** represents 1,000 noisy orbits starting from the corresponding perturbed state, while each point in **(c, d)** represents 10 such orbits for each of the 100 network realizations of the given network size. In every case, the approach to the target can thus be insulated against noise with a slight modification of the compensatory perturbation procedure, thereby preserving its effectiveness.



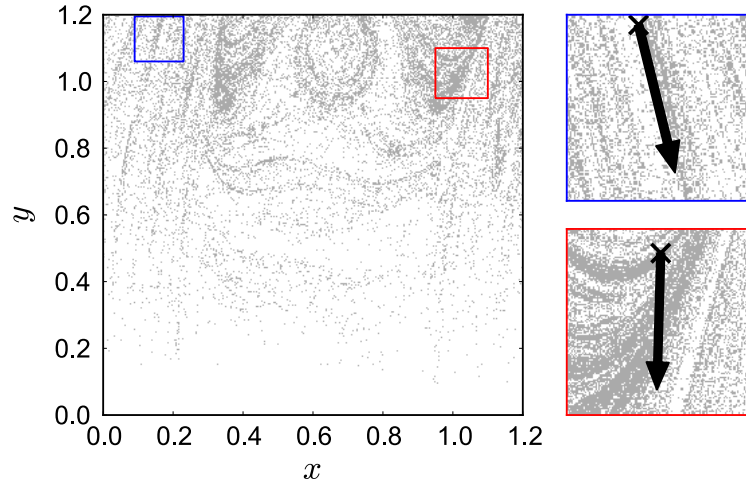
Supplementary Figure S3: Robustness of compensatory perturbations against parameter uncertainty. (a, b) Bars denote the success rate of candidate compensatory perturbations in directing network to the target, for the compensatory perturbations predicted by our original computational procedure (red) and the modified compensatory perturbations as described in the Supplementary Discussion (grey). Each set of bars represents a sample of 1,000 random networks and initial and target states as considered in Supplementary Figure S7, and the success rate for each of these networks is an average over 100 randomized parameter sets in which we allow every parameter of the system to vary independently and uniformly within a range of $\pm 5\%$ about its nominal value. In both cases, the significantly higher success rate for the modified perturbations demonstrates that failure to control the system is buffered against parameter uncertainty by driving the system further inside the target basin. (c, d) Distribution of distances between the target state of the original network and the corresponding stable state of the networks with modified parameters considered in panels (a) and (b), respectively. The distances are normalized by the (common) equilibrium value of the dynamical units in the target state \bar{x}_B (compare with Supplementary Fig. S7a).



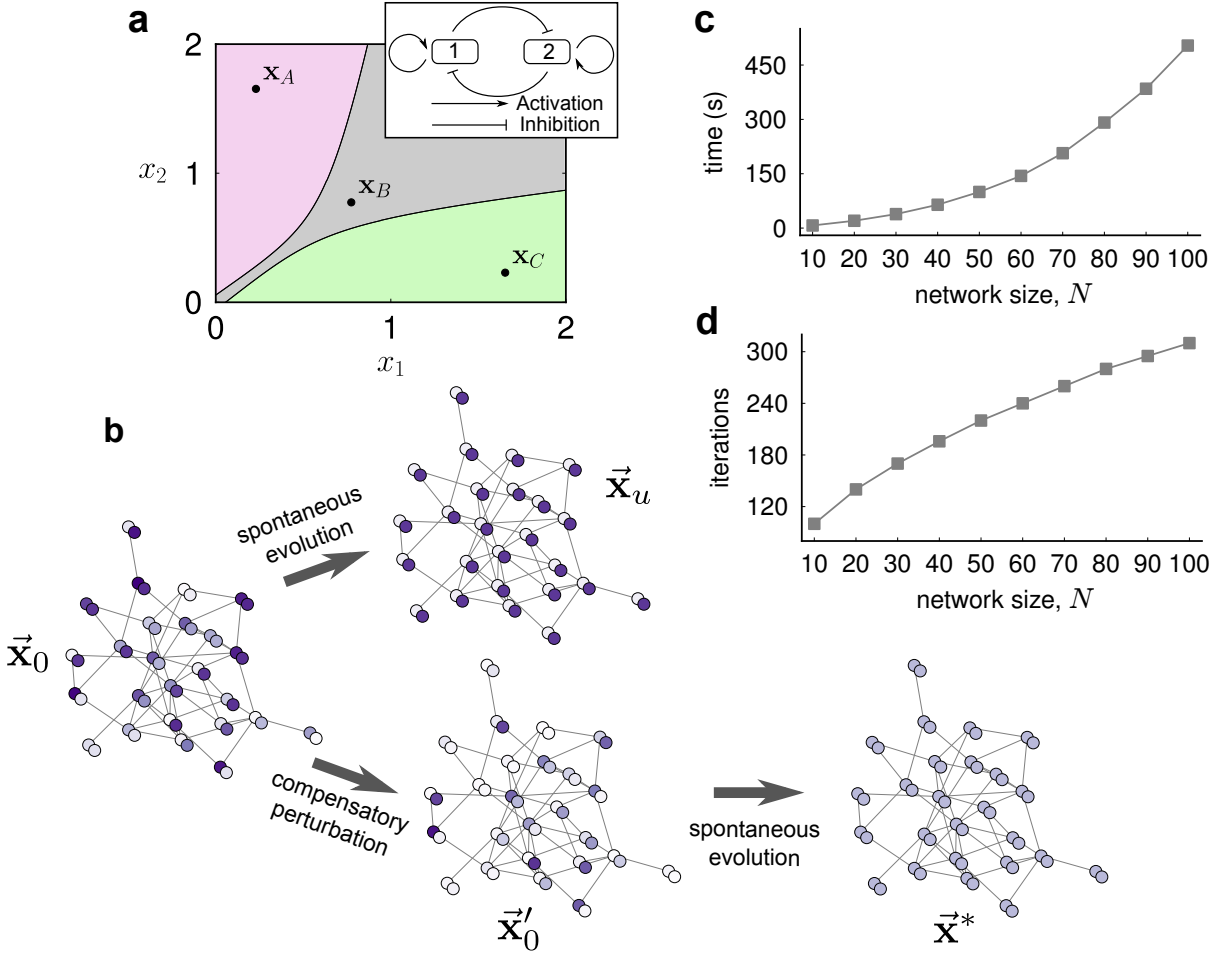
Supplementary Figure S4: Illustration of the control process in two dimensions. Yellow and blue represent the basins of attraction of the stable states x_A and x_B , respectively, while white corresponds to unbounded orbits. **(a, b)** Iterative construction of the perturbation for an initial state in the basin of x_A with x_B as a target **(a)**, and for an initial state on the right side of both basins with x_A as a target **(b)**. Dashed and continuous lines indicate the original and controlled orbits, respectively. Red arrows indicate the full compensatory perturbations. Individual iterations of the process are shown in the insets (for clarity, not all iterations are included).



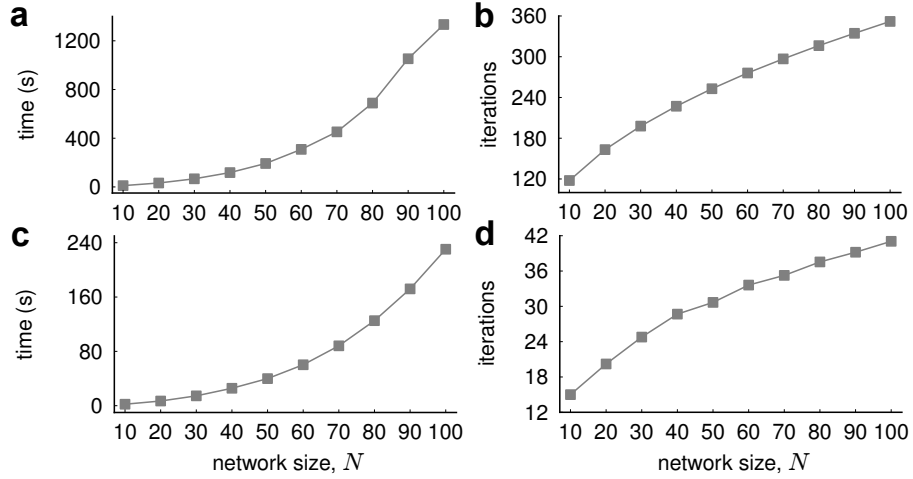
Supplementary Figure S5: Examples of compensatory perturbations in a system with fractal basins. Section of the state space of eq. (S1) at $t = 0 \pmod{2\pi}$. The basins of the clockwise (\mathbf{x}_+) and counterclockwise (\mathbf{x}_-) attractors are colored grey and white, respectively. The basins were calculated by sampling the pictured portion of the state space at a resolution of 1,000 points along each coordinate direction. The points at which the attractors strike the plane, which are taken as the corresponding target states within our method, are marked with a red and blue \times , respectively. The right panels show examples of compensatory perturbations found by our method that take an initial condition (black \times) in the basin of \mathbf{x}_- and move it to the basin of \mathbf{x}_+ (red), and vice versa (blue).



Supplementary Figure S6: Examples of compensatory perturbations in a system with riddled basins. Section of the state space of eq. (S2) through $\dot{x} = \dot{y} = t \bmod \frac{2\pi}{\omega} = 0$. Initial conditions corresponding to unbounded orbits ($|y| \rightarrow \infty$) are shaded in grey. The basin of attraction of the chaotic attractor that lies in the subspace defined by $y = \dot{y} = 0$ appears in white. Initial conditions were sampled at a resolution of 1,000 points along each coordinate direction. The right panels show two examples of compensatory perturbations found by our method that take initial conditions corresponding to unbounded orbits (black \times) and drive them into the basin of the chaotic attractor.



Supplementary Figure S7: Control of large random networks. (a) State space of the two-gene subnetwork represented in the inset, where the curves mark the boundaries between the basins of x_A , x_B , and x_C . (b) Illustration of compensatory perturbation on the genetic networks described by equation (S5), where each node is a copy of the two-gene system. We are given an initial network state \vec{x}_0 representing the expression levels of the N gene pairs (color coded), and this state evolves to a stable state of the network \vec{x}_u (top path). The goal is to knockdown one or more genes to reach a new state \vec{x}'_0 that instead evolves to a target stable state $\vec{x}^* \neq \vec{x}_u$ (bottom path). (c, d) Average computation time (c) and average number of iterations (d) required to control networks of N nodes with initial state $\vec{x}_0 = \vec{x}_A$ and target $\vec{x}^* = \vec{x}_B$, demonstrating the good scalability of the algorithm. Each point represents an average over 1,000 independent random network realizations.



Supplementary Figure S8: Efficiency for alternate initial and target states. Counterparts to Supplementary Figure S7c-d for: **(a, b)** initial state $\vec{x}_0 = \vec{x}_A$, target state $\vec{x}^* = \vec{x}_C$; and **(c, d)** initial state $\vec{x}_0 = \vec{x}_B$, target state $\vec{x}^* = \vec{x}_A$. The other combinations of initial and target states involving \vec{x}_A , \vec{x}_B , and \vec{x}_C follow from these ones and the one in Supplementary Figure S7c-d by symmetry. The approximately $N^{5/2}$ dependence of the computation time and sublinear dependence of the number of iterations are largely independent of the particular initial and target states under consideration.

Supplementary Table

Supplementary Table S1: Control procedure parameter values. The relevant parameters are the integration time (τ) and tolerance (κ) used to test convergence to the target state, the limit on the number of iterations (I), the lower (ϵ_0) and upper (ϵ_1) bounds on the size of each incremental perturbation, and the time window (T) over which the closest approach to the target is identified.

	τ	κ	I	ϵ_0	ϵ_1	T
T Cell signaling network	10^3	10^{-2}	10^4	10^{-3}	10^{-2}	5
Associative memory network	2×10^2	10^{-2}	10^4	10^{-3}	10^{-2}	10
New England power grid	10^3	10^{-1}	10^4	10^{-2}	10^{-1}	10
2D potential system	10^4	10^{-2}	10^3	10^{-3}	10^{-2}	10
Random genetic networks	10^4	10^{-2}	10^4	5×10^{-3}	5×10^{-2}	10

Supplementary Methods

Termination criteria and control parameters. The control procedure is terminated if the updated initial condition attracts to within a distance κ of the target state within τ time units. Otherwise, we terminate the search if a compensatory perturbation is not found after a fixed number I of iterations. In general, this number should be of the order of L/ϵ_0 , where L is the characteristic linear size of the feasible region. For each iteration, we use T time units within the integration step that identifies t_c , which was estimated based on the time to approach the undesirable stable state. As described in the main text, the parameters ϵ_0 and ϵ_1 define the minimum and maximum size of the incremental perturbation within the optimization step, respectively. Table S1 lists the parameter values used for each of the systems we have studied.

In all systems we have studied, when a solution cannot be found, this is manifested in our method as an inability to move the orbit any closer to the target, which eventually leads to oscillations within the feasible region. The parameter I is always taken to be large enough that this occurs before the iteration limit is reached. This also points to an alternative formulation of the termination criterion in which the procedure is terminated if it revisits an initial condition \mathbf{x}'_0 from a prior iteration within a distance less than ϵ_0 .

Construction of random genetic networks. The networks used in the Supplementary Discussion are grown starting with a d -node connected seed network, by iteratively attaching a new node and connecting this node to each pre-existing node i with probability $d \times P_i$, where $\sum_i P_i = 1$. The connections are assumed to be unweighted and undirected. We reject any iteration resulting in a degree-zero node, thereby ensuring that the final N -node network is connected and has average degree $> 2d$ for large N . Networks are generated with uniform attachment probability, where $P_i = 1/N^{(q)}$ and $N^{(q)}$ is the number of nodes in the network at iteration q . In our simulations, we focused on networks with $d = 2$.

Drawbacks of alternative implementations. The method introduced in the main text should be compared with a number of apparently simpler implementations that could, in principle, be used to search the network state space for the purposes of finding a compensatory perturbation. For example, rather than keeping track of the variational matrix $\mathbf{M}(\mathbf{x}_0, t)$, which requires the integration of n^2 additional differential equations at every iteration, one could imagine using backward integration of a trajectory starting at $\mathbf{x}(t_c) + \delta\mathbf{x}(t_c)$ to identify a suitable initial perturbation. This alternative procedure suffers the critical drawback that, for a particular choice of $\delta\mathbf{x}(t_c)$ (magnitude and direction), it is not certain that the time-reversed orbit will ever strike the feasible region defined by equation (2) (main text). This is particularly so in realistic situations where only a fraction of the nodes are accessible to perturbations, resulting in a feasible region of measure zero in the full n -dimensional state space.

Similar in spirit to our approach are standard shooting or “shoot-and-look” type methods, which seek to solve an initial value problem such that it satisfies a particular boundary condition (in this case, reaching the target at time τ). These methods operate by making repeated adjustments to the initial condition \mathbf{x}_0 , observing how those adjustments change the orbit at a later time, and then keeping those adjustments that move the orbit closer to the intended boundary value. The problem is that in each step, in order to “look” we must first “shoot”, which requires an expensive integration of the system dynamics. Our approach circumvents this by calculating the mapping between *all* (small) initial perturbations and their images at later times (the variational matrix M), which allows us to determine the optimal “shot” at every iteration with only one integration. Similar problems afflict other techniques that involve random adjustment and then updating of data, such as simulated annealing. In the high-dimensional state spaces typical of real networks, each successful update of the initial condition within these methods simply requires too many trial sub-iterations, each of which entails evolving the system dynamics.

Supplementary Discussion

Illustration of control procedure in two dimensions. It is instructive to apply the control procedure introduced in the main text to an example in two dimensions, where the basins of attraction (and hence the possible compensatory perturbations) can be explicitly calculated and visualized. Supplementary Figure S4 shows the state space of the system, which has two stable states, \mathbf{x}_A on the left and \mathbf{x}_B on the right. The system consists of a particle in one dimension under the influence of the potential $U(x_1) = \exp(-\gamma x_1^2)(bx_1^2 + cx_1^3 + dx_1^4)$ and frictional dissipation η , where $\gamma = 1$, $b = -1$, $c = -0.1$, $d = 0.5$, $\eta = 0.1$, and $x_2 = \dot{x}_1$. The method is illustrated for two different initial states under the constraint that admissible perturbations have to satisfy $\mathbf{x}'_0 \leq \mathbf{x}_0$, i.e., one cannot increase either variable.

For the initial state in the basin of state \mathbf{x}_A (Supplementary Fig. S4a), no admissible perturbation exists that can bring the system directly to the target \mathbf{x}_B , on the right, since that would require increasing x_1 . However, our iterative procedure builds an admissible perturbation vector that shifts the state of the system to a branch of the basin $\Omega(\mathbf{x}_B)$ lying on the left of that point. Then, from that instant on the autonomous evolution of the system will govern the trajectory's approach to the target \mathbf{x}_B , on the right. This example illustrates how compensatory perturbations that move in a direction away from the target—the only ones available under the given constraints—can be effective in controlling the system, and how they are identified by our method. The other example shown illustrates a case in which the perturbation to an initial state on the right crosses an intermediate basin, that of \mathbf{x}_B , before it can reach the basin of the target, \mathbf{x}_A (Supplementary Fig. S4b). The linear approximation fails at the crossing point, but convergence is nonetheless assured by the constraints imposed on $\delta\mathbf{x}_0$ (*Methods*). Our method is similarly capable of dealing with even more complicated basin structures, such as fractal or riddled basins (see *Effectiveness of control in the presence of fractal basins* and *Effectiveness of control in the presence of riddled basins* below). For a step-by-step animation of the control procedure in this system, please refer to Supplementary Movie.

Effectiveness of control in the presence of fractal basins. Systems with fractal basin boundaries may in principle be a challenge for our approach due to the possible existence of very long transients before the orbit comes near the relevant attractor. To test our approach's ability to cope with this scenario, we have applied it to a well-known system exhibiting fractal basins, namely, a driven, dissipative oscillator, whose dynamics obey

$$\frac{d^2\theta}{dt^2} + \nu \frac{d\theta}{dt} + \sin \theta = F \cos t, \quad (\text{S1})$$

where θ denotes the phase of the oscillator and the values of the damping parameter ($\nu = 0.1$) and forcing parameter ($F = 2.1$) are taken from [29]. We identify a unique state within the three-dimensional state space of this system by $\mathbf{x} = (x_1, x_2, x_3) = (\theta, \dot{\theta}, t)$, where the dot denotes a time

derivative. This system possesses two periodic attractors each with period 2π and distinguished by average clockwise or counterclockwise motion ($\langle \dot{\theta} \rangle$ positive or negative). We denote these attractors by $\mathbf{x}_+(t)$ and $\mathbf{x}_-(t)$, respectively. A section of the state space at $t = 0 \pmod{2\pi}$ is shown in Supplementary Figure S5, with the two (fractal) basins of attraction shaded. Given an initial state $\mathbf{x}_0 = (\theta_0, \dot{\theta}_0, 0)$ in the basin of one attractor, we attempt to use our method to find a compensatory perturbation that places the system in the basin of the other attractor. We use as a target state the point on the other attractor at $t = 0 \pmod{2\pi}$. Since we are primarily concerned with our method’s ability (or inability) to find compensatory perturbations within the convoluted state space, the only constraint we apply is that eligible perturbations cannot adjust the artificial coordinate $x_3(0)$ that represents time. Note that since the dynamics are invariant under translation of either θ or t by 2π , we measure differences along these coordinate directions modulo 2π for the purposes of the distance metric used in our method. We use the conservative parameter choices of $\epsilon_0 = 10^{-4}$, $\epsilon_1 = 10^{-3}$, $\kappa = 10^{-3}$, $I = 100,000$, $\tau = 100 \times 2\pi$, and $T = 2\pi$. The integration time window T is deliberately chosen to be short (only one period) as a test of the importance of long transients. In other words, our method will only consider a short initial portion of the orbit in deciding how to proceed at every iteration.

The right panels of Supplementary Figure S5 show the results of two control experiments, taking an initial point in the basin of $\mathbf{x}_-(t)$ and targeting $\mathbf{x}_+(t)$, and vice versa. Our method successfully finds states in the target basin in both cases, and with little apparent difficulty—only a few hundred iterations are required in either case, and we observe that the method makes more or less consistent progress moving the orbit closer to the target. While we have shown only two examples for clarity, these results are representative of 1,000 initial states, chosen randomly from the phase plane of Supplementary Figure S5, each of which we attempt to bring to the opposite basin. Remarkably, our method is successful in over 99% of these cases. We posit that long transients are not an issue because it is not critical that the uncontrolled orbit come “near” the target, in any absolute sense. Rather, all that is necessary is a point on the orbit at which progress can be made through an incremental perturbation. In the worst case, a long transient simply means one must evolve the system dynamics for a longer time to verify which attraction basin the current initial condition belongs to.

Effectiveness of control in the presence of riddled basins. Another complicated basin structure that can arise in special cases is a so-called *riddled* basin, in which every point in the basin has points of a different basin arbitrarily closeby (the basin is “riddled” with holes). While this property could in principle pose problems for the identification of compensatory perturbations, we verified that our approach can perform quite well in such systems. This is the case because, as for other attractors, these basins too have non-zero measure in the state space. We used a most widely-known system with a riddled basin introduced in ref. 62. The system consists a point particle of unit mass moving in two dimensions $\mathbf{r} = (x, y)$ under the influence of the potential $V(x, y) =$

$(1 - x^2)^2 + (x + \bar{x})y^2$, with dynamics governed by

$$\frac{d^2 \mathbf{r}}{dt^2} = -\nabla V + \mathbf{e}_x f_0 \sin \omega t - \nu \frac{d\mathbf{r}}{dt}, \quad (\text{S2})$$

where the second and third terms represent the influences of a driving force and friction, respectively, and \mathbf{e}_x is a unit vector in the x direction. We represent a point within the five-dimensional state space by $\mathbf{x} = (x, \dot{x}, y, \dot{y}, t)$ and use the parameter values $f_0 = 2.3$, $\omega = 3.5$, $\bar{x} = 1.9$, and $\nu = 0.05$ given in ref. 62. For these parameters, this system possesses a chaotic attractor $\mathbf{x}_A(t)$ in the subspace defined by $y = \dot{y} = 0$, whose basin is riddled with initial conditions corresponding to unbounded orbits ($|y| \rightarrow \infty$). A (x_0, y_0) slice of the state space showing the riddled basin structure is depicted in Supplementary Figure S6 for $\dot{x} = \dot{y} = t = 0$. Given an initial condition in this plane corresponding to an unbounded orbit (grey), we attempt to use our method to bring it to the basin of attraction of the chaotic attractor (white) by perturbing only the coordinates x_0 and y_0 . Since the desired attractor is an extended set in this case, we use a single point on the attractor (namely $(x, \dot{x}, t) = (-0.991, -1.254, 1000)$) as the target state within our method, which is not directly reachable by any eligible perturbation. Nonetheless, our method is 100% successful within a sample of 1,000 initial states selected randomly from the unbounded “basin” depicted in Supplementary Figure S6. The parameters used for the control procedure in this analysis were $\epsilon_0 = 10^{-4}$, $\epsilon_1 = 10^{-3}$, $\kappa = 10^{-3}$, $I = 100,000$, $\tau = 1000$, and $T = 10$.

Effectiveness and computational efficiency. In order to validate our procedure for identifying compensatory perturbations in networks, we consider networks of diffusively-coupled units—a case that has received much attention in the study of spontaneous synchronization⁴⁷. We take as a base system the genetic regulatory subnetwork shown in Supplementary Figure S7a (inset), consisting of two genes wired in a circuit. The state of the system is determined by the expression levels of the genes, represented by the variables $x_1, x_2 \geq 0$. The associated dynamics obeys

$$\frac{dx_1}{dt} = a_1 \frac{x_1^m}{x_1^m + S^m} + b_1 \frac{S^m}{x_2^m + S^m} - k_1 x_1 + f_1, \quad (\text{S3})$$

$$\frac{dx_2}{dt} = a_2 \frac{x_2^m}{x_2^m + S^m} + b_2 \frac{S^m}{x_1^m + S^m} - k_2 x_2 + f_2, \quad (\text{S4})$$

where the first two terms for each gene capture the self-excitatory and mutually inhibitory interactions represented in Supplementary Figure S7a, respectively, while the final two terms represent linear decay ($k_{1,2}$) and basal activation ($f_{1,2}$) rates of the associated gene’s expression. The parameter S represents the threshold above (below) which each gene is considered “on” (“off”). While used here as a benchmark to test our computational approach, it is worth noting that models of this form have been employed to describe the transition between progenitor stem cells and differentiated cells^{40,48,49}, and that genetic “switch” circuits have been recognized as important motifs for the control of biochemical networks⁵⁰. For a wide range of parameters, this system exhibits three

stable states: a state (\mathbf{x}_B) characterized by comparable expression of both genes, and two states (\mathbf{x}_A and \mathbf{x}_C) characterized by the dominant expression of one of the genes. The former corresponds to a stem cell state, and the latter correspond to two distinct differentiated cell types. Supplementary Figure S7 and subsequent results correspond to the symmetric choice of parameters $a_{1,2} = 0.5$, $b_{1,2} = 1$, $k_{1,2} = 1$, $f_{1,2} = 0.2$, $S = 0.5$, and $m = 4$. We assume that compensatory perturbations are limited to decreases in gene expression, i.e., $\mathbf{x}'_0 \leq \mathbf{x}_0$. Our procedure applied to this system identifies compensatory perturbations between all three stable states (Supplementary Movie).

We construct large networks by coupling multiple copies of the two-gene system described above (Supplementary Methods). Such intercellular genetic networks may represent cells in tissue or culture coupled by means of factors exchanged through their microenvironment or medium. Specifically, we assume that each copy of the genetic system in equations (S3)-(S4) can be treated as a node of the larger network. The dynamics of a network consisting of N such systems is then governed by

$$\frac{d\mathbf{x}_i}{dt} = \mathbf{f}(\mathbf{x}_i) + \frac{\sigma}{d_i} \sum_{j=1}^N A_{ij}[\mathbf{x}_j - \mathbf{x}_i], \quad (\text{S5})$$

where $\dot{\mathbf{x}}_i = \mathbf{f}(\mathbf{x}_i)$ is the vectorial form of the dynamics of node i as described by equations (S3)-(S4), the parameter $\sigma > 0$ is the overall coupling strength, and d_i is the degree (number of connections) of node i . The structure of the network itself is encoded in the adjacency matrix $A = (A_{ij})$. We use $\vec{\mathbf{x}} = (\mathbf{x}_i)$ to denote the state of the network, with $\vec{\mathbf{x}}_A$, $\vec{\mathbf{x}}_B$, and $\vec{\mathbf{x}}_C$ denoting the network states in which all nodes are at state \mathbf{x}_A , \mathbf{x}_B , and \mathbf{x}_C , respectively. The states $\vec{\mathbf{x}}_A$, $\vec{\mathbf{x}}_B$, and $\vec{\mathbf{x}}_C$ are fixed points of the full network dynamics in the $2N$ -dimensional state space and, by arguments of structural stability, we can conclude they are also stable and have qualitatively similar basins of attraction along the coordinate planes \mathbf{x}_i if the coupling strength σ is weak. While we focus on these three states, it follows from the same arguments that in this regime there are $3^N - 3$ other stable states in the network. Under such conditions, compensatory perturbations between $\vec{\mathbf{x}}_A$, $\vec{\mathbf{x}}_B$, and $\vec{\mathbf{x}}_C$ are guaranteed to exist, and hence this class of networks can also serve as a benchmark to test the effectiveness and efficiency of our method in finding compensatory perturbations in systems with a large number of nodes.

A general compensatory perturbation in this network is illustrated in Supplementary Figure S7b, where different intensities indicate different node states. Applied to the initial state $\vec{\mathbf{x}}_A$ and target $\vec{\mathbf{x}}_B$ for $\sigma = 0.05$, the method is found to be effective in 100% of the cases for the 10,000 networks tested, with N ranging from 10 to 100. Moreover, the computation time and number of iterations for these tests confirm that our method is also computationally efficient for large networks. Computation time grows polynomially with N (Supplementary Fig. S7c), as expected since each iteration requires the integration of $O(N^2)$ equations and each equation can be integrated in $O(1)$ time as long as the average degree remains essentially constant, as is the case in many network models. The number of iterations grows as the square root of N (Supplementary Fig. S7d), in agreement with the \sqrt{N} scaling of $|\vec{\mathbf{x}}_A - \vec{\mathbf{x}}_B|$ and of the distances between other invariant sets. This

leads to the asymptotic scaling $N^{5/2}$ for the computation time. These properties are representative of other choices of initial and target states (Supplementary Fig. S8). Note that our argument for the time complexity does not depend on the particular functional form of the dynamics nor on any parameter other than the dimension of the state space (which is usually proportional to the number N of nodes, as assumed here).

Comparison with existing literature. Note that our approach is fundamentally different from those usually considered in control theory, both in terms of methods and applicability. To appreciate this, it is instructive to compare the problem addressed here—and the solution offered—to other important problems that fall under the broad umbrella of “control”.

One well-developed meaning of “control” entails the optimization of specific system properties. Optimal control⁵¹, for example, is based on identifying an admissible (time-dependent) control signal $\mathbf{u}(t)$ such that an orbit of the modified system $d\mathbf{x}/dt = \mathbf{G}(\mathbf{x}, \mathbf{u}, t)$ will optimize a given cost functional $J(\mathbf{x}, \mathbf{u})$. In this representation, the discrete interventions we consider would take the form $\mathbf{u}(t) = \mathbf{u}_0\delta(t - t_0)$, where \mathbf{u}_0 is then a compensatory perturbation to be determined. At first glance then, the discrete form of the controls we seek is the same as those used in impulse control⁵². But we stress that here, the challenge is not to identify an “optimal” solution but a *valid* solution in the first place (*i.e.*, an eligible point $\mathbf{x}_0 + \mathbf{u}_0$ inside the target’s basin of attraction). This is a goal that cannot be easily guided by global optimization of any particular “cost” in a computationally tractable way, nor formulated simply as one or more closed form (in)equality constraints. For this reason, the extensive and well-developed machinery of optimal control, impulse control, model predictive control, and related methodologies unfortunately cannot be directly applied to solve the problem considered here.

Another important sense of “control” concerns the stabilization of otherwise unstable (and therefore uninhabitable) states. Control of chaos⁵³, for instance, can be used to convert a chaotic trajectory into a periodic one, and is based on the continuous application of unconstrained small time-dependent perturbations to align the stable manifold of an unstable periodic orbit with the trajectory of the system. Similar methods have been applied, for example, to stabilize desirable periodic behaviors in models of cardiac activity⁵⁴. Conversely, techniques have also been developed to destroy undesirable attractors by using an appropriate modulation of the system parameters^{55,56}. Here, however, we do not seek to create or annihilate a stable state, but rather to bring the system to an existing state that is already stable. Moreover, we seek to do this using one (or few) constrained finite-size perturbations to the system *state* (rather than the dynamical system itself), and these perturbations are forecast-based rather than feedback-based.

More similar to the sense of “control” that we consider here is the method of targeting⁵⁷, which can be used to facilitate the approach to a desired orbit. But like control of chaos, this method generally applies when one wishes to move within the same ergodic component rather than to move between different basins of attraction as we do here. And although a few methods

have been developed to accomplish such transitions in multiple-attractor systems, they generally require prior knowledge about features of the network state space either directly⁵⁸ or indirectly via auxiliary techniques such as Lyapunov functions⁵⁹. This unfortunately limits their applicability to low-dimensional systems and special cases for which such information is available. Indeed, the central challenge that our approach seeks to overcome is the identification of control interventions without reliance on details of global properties of the state space of the network in question.

A closer precedent to our work is ref. 12, where examples of compensatory perturbations were provided for food-web networks. They were identified, however, by seeking to make the current state of the system similar to a desired state. Such heuristics do not directly account for the subsequent time evolution of the perturbed orbit (i.e., the control perturbation is not forecast based) and they do not take systematic advantage of the critical role of basins of attraction, which, as demonstrated here, allow control even when the target itself is not directly accessible. It should also be noted that while our approach makes use of constrained optimization⁶⁰, the question at hand cannot be formulated as a simple optimization problem in terms of an aggregated objective function, such as the number of active nodes. Maximizing this number by ordinary means can lead to local minima or transient solutions that then fall back to asymptotic states with a larger number of inactive nodes. The identification of stable states that enjoy the desired properties is thus an important step in our formulation of the problem.

None of this is to suggest that the other methodologies discussed in this section are in any way deficient. As we have noted, they simply address different problems from the one considered here. Our formulation of the control problem can nonetheless benefit from existing techniques. Once a compensatory perturbation has been found, existing control and optimization methods can be used to modify this solution so as to optimize specific properties. For example, it might be of interest to identify a solution that, among all eligible ones, brings the system to the target the fastest. Incidentally, for lying further inside the target basin of attraction, such solutions have the remarkable property of being resilient against noise and parameter uncertainty (see *Effects of stochasticity* and *Effects of parameter uncertainty* below, Supplementary Figs. S1-S3). These possibilities underscore the robustness and versatility of our core approach. We emphasize, however, that alternative compensatory perturbations can only be found with existing methods once at least one eligible state inside the target basin has already been identified.

Effects of stochasticity. In our formulation of the network control problem and our procedure for identifying compensatory perturbations, we have assumed the network dynamics is deterministic. In real systems, however, there will often be noise in the dynamics. This raises the question of whether our approach can be used to effectively control systems with a stochastic component. To address this question, we revisit here the compensatory perturbations predicted with our method on deterministic models, and test their effectiveness in a noisy version of the same system. We do this for *i*) the mechanical example system presented in Supplementary Figure S4, and *ii*) the genetic

network model with the initial/target states considered for Supplementary Figure S7. To model the effects of stochasticity, we include an additive noise term in the dynamics of each state variable, yielding the stochastic differential equation $dx/dt = \mathbf{F}(\mathbf{x}) + \xi(t)$ for the new dynamics. Following the notation in the main text, \mathbf{F} is the n -dimensional deterministic dynamics, and $\xi(t)$ is a vector of n independent Gaussian white noise processes, each with mean 0 and r.m.s. amplitude s (which quantifies the strength of the noise). Starting from a state \mathbf{x}'_0 reached by a putative compensatory perturbation, we generate many independent realizations of the noisy dynamics using a stochastic Runge-Kutta scheme⁶¹ to determine the probability that the noisy system reaches the target.

Before we proceed with a numerical experiment, we must appropriately define the notions of “stability” and “attractors” in the presence of stochasticity, since with the addition of noise fixed points are no longer strictly fixed. We consider a noisy orbit to reach the target if, after the usual integration time limit τ used to test convergence to the target in the deterministic case (Supplementary Methods), the mean position $\langle \mathbf{x}(t) \rangle$ over an additional 1,000 time units falls within a ball of radius r around the target. We then consider noise strengths s up to a maximum s_{\max} , where the threshold s_{\max} is defined such that at this noise level the standard deviation of the noisy orbit around the target in any direction is at most r . Rigorously, we consider the stochastic dynamics near the target state \mathbf{x}^* , given by $dx/dt = A \cdot \mathbf{x} + s \xi(t)$, where $A = D_{\mathbf{x}}\mathbf{F}|_{\mathbf{x}^*}$ is the Jacobian matrix of \mathbf{F} evaluated at the target state. Over long times, the maximum expected variance of this process along any coordinate direction is $\sim s^2/(2|\lambda_{\min}|)$, where s is the noise strength as defined above and λ_{\min} is the real part of the eigenvalue of A with smallest real part magnitude. Thus, our criterion for the noise strength s_{\max} that defines a fuzzy “ball of stability” of radius r around the target is $s_{\max} = \sqrt{2r|\lambda_{\min}|}$. We use $r = 0.1$ for the systems in this section, which yields $s_{\max} \approx 0.02$ and $s_{\max} \approx 0.03$ for the two-dimensional mechanical system and random genetic network systems, respectively.

Supplementary Figure S1a-b illustrates the effect of noise for the compensatory perturbations presented in Supplementary Figure S4a-b, respectively. Although the concept of a “basin of attraction” is not absolute in the presence of noise, it is instructive to interpret the effects of noise in terms of how it might “kick” the orbit between the deterministically-defined basins—regions where the mean dynamics tends toward one attractor or the other. Indeed, because our algorithm declares success after finding a point \mathbf{x}'_0 just inside the target’s basin of attraction, it is possible for the noisy trajectory to wander back across the boundary into the basin of the other attractor (red curves). But there is nothing in our formulation of the control problem that dictates we must perturb the system to any particular point \mathbf{x}'_0 ; in general, there will exist other eligible states *further inside* the target’s basin of attraction. By instead choosing one of those points, \mathbf{x}''_0 , as the endpoint of our compensatory perturbation, the resulting orbit is far more likely to stay within the deterministic target basin and as a result, far more likely to reach the target (grey curves).

Systematically, we choose the modified perturbed state \mathbf{x}''_0 by starting from $\mathbf{x}'_0 = \mathbf{x}'_0$ and minimizing the time $T(\mathbf{x}''_0)$ it takes the deterministic orbit resulting from \mathbf{x}''_0 to reach a neighbor-

hood of the target, namely, the same criterion used for attraction in the main text. Any such state \mathbf{x}_0'' must also comply with the given constraints on the eligible compensatory perturbations defined by $\mathbf{g}(\mathbf{x}_0, \mathbf{x}_0'')$ and $\mathbf{h}(\mathbf{x}_0, \mathbf{x}_0'')$. This is done according to the nonlinear programming problem

$$\begin{aligned} \min_{\mathbf{x}_0''} \quad & T(\mathbf{x}_0'') \\ \text{s.t.} \quad & \mathbf{g}(\mathbf{x}_0, \mathbf{x}_0'') \leq 0 \\ & \mathbf{h}(\mathbf{x}_0, \mathbf{x}_0'') = 0. \end{aligned} \tag{S6}$$

This problem can be solved by existing methods, and we implement it using Sequential Quadratic Programming (Methods) immediately after the application of our control procedure that identifies \mathbf{x}_0' . Since this problem is a single optimization of a continuous and well-defined objective function, this additional step is not costly. But note that solving the problem given by equation (S6) in such a straightforward way is possible only because we have solution \mathbf{x}_0' that belongs to the basin of the target and hence reaches the vicinity of the target in finite time.

Supplementary Figure S2a-b is a numerical demonstration of the effectiveness of the above procedure, for the respective control scenarios represented by the initial/target state combinations in Supplementary Figure S4a-b. As the strength of the noise term is increased, the success rate of the original compensatory perturbations in both scenarios quickly drops to $\approx 50\text{-}60\%$ (red). As shown in Supplementary Figure S1, this can be attributed to the initial state's proximity to the boundary between the basins of \mathbf{x}_A and \mathbf{x}_B , which allows noise to knock the orbit back and forth between the attraction basins. (Because the state \mathbf{x}_0' is slightly inside the target basin, this process is biased, yielding a success rate above 50%). Nevertheless, the slight modification described above yields initial conditions \mathbf{x}_0'' that are significantly more likely to reach their respective targets at all noise levels (grey), with success rates of $\approx 70\%$ (Supplementary Fig. S2a) and $\approx 90\%$ (Supplementary Fig. S2b) at the maximum noise strength. This is even more pronounced in the network case (Supplementary Fig. S2c-d), where the effectiveness of the original compensatory perturbations degrades quickly with increasing noise, particularly in larger networks. This precipitous drop in the success rate is a consequence of the large number of attractors (3^N) in this model, which makes the effect of noise near the corresponding basin boundaries analogous to flipping a many-sided coin to determine the ultimate fate of the network. These seemingly prohibitive odds highlight the resilience offered by our formulation of the network control problem. By moving the system further inside the desired basin, namely to \mathbf{x}_0'' , the modified interventions ensure that the system will reach the target in nearly 100% of cases up to near the maximum noise strength, even when the network size is increased.

Effects of parameter uncertainty. To formalize our approach in terms of the system's state space, we have assumed a model describing the dynamics of the system under study. Such a model usually contains a (potentially large) number of parameters, and in practice the values of these parameters may not be known precisely. A potential problem confronting our approach is thus that, when

predicted using an imperfect model, a compensatory perturbation may place the real system in a different basin of attraction than the one intended.

To address this possibility, we performed the following analysis. We consider the genetic network model as used in Supplementary Figure S7, with weak coupling and the respective initial and target states taken to be $\vec{x}_0 = \vec{x}_A$ and $\vec{x}^* = \vec{x}_B$. For all nodes, we use the nominal values of the parameters $a_{1,2}$, $b_{1,2}$, $k_{1,2}$, $f_{1,2}$, S , and m presented in the main text. Given a network with these parameters, we predict two interventions: the original compensatory perturbation $\mathbf{x}_0 \rightarrow \mathbf{x}'_0$ found by our method, and a modified perturbation $\mathbf{x}_0 \rightarrow \mathbf{x}''_0$ given as a solution to the problem described by equation (S6); like in our study of the effects of stochasticity above, \mathbf{x}''_0 is by design further inside the predicted target basin. Now, suppose that the nominal parameter values do not accurately represent the real system being modeled, and that the actual parameters lie somewhere in a window of uncertainty about their nominal values, which we take to be $\pm 5\%$ in our numerical experiments. Furthermore, suppose each of the six aforementioned parameters is allowed to vary in this way *independently* for each node, meaning that the coupled subsystems are no longer identical. We then test whether the predicted perturbations still drive the system to the target when the parameters have been altered to the actual values. We calculate the success rate of each perturbation across a number of these alternate parameter sets, chosen randomly within the range defined above. Supplementary Figure S3a-b shows the results for networks of sizes 10 and 20, respectively. Although the original perturbation often fails to bring the system to the target when the actual parameters differ from their nominal values (red bars), the modified perturbations succeed nearly 100% of the time (grey bars), despite having been predicted based on a model that is ostensibly “wrong”.

Note that a change in the system parameters usually induces a change in the system’s state space as well, including the location, stability, and very existence of the fixed points. Thus, in all networks considered above, the target state is displaced from its location in the imperfect model. We find the appropriate target state based on Newton’s method applied to the dynamics of the exact model, starting from the target state determined in the imperfect model as an initial guess. Any parameter assignment for which this procedure does not yield a stable fixed point in the positive orthant for the new target is rejected. This is a minor restriction, especially in light of the fact that most models are construed to faithfully reproduce the equilibria of interest. Supplementary Figure S3c-d shows the distribution of the amount the target moves for the eligible parameter choices within the uncertainty window we consider.

Here, as for the effect of noise considered above, we have shown that there is a simple, computationally inexpensive way to make the approach resilient against imperfections in the modeling. Both problems are addressed by a slight adjustment to our basic method, namely, moving the system further inside the predicted target basin by systematically minimizing the time taken to reach the target state. We emphasize that this is possible because our formulation of the network control problem is based on taking advantage of extended features of the state space, such as basins of attraction. In this way, the challenges posed by stochasticity and parameter uncertainty highlight

robustness as a fundamental strength of our approach.

Supplementary References

47. Pecora L. M. & Carroll T. L. Master stability functions for synchronized coupled systems. *Phys. Rev. Lett.* **80**, 2109–2112 (1998).
48. Roeder I. & Glauche I. Towards an understanding of lineage specification in hematopoietic stem cells: a mathematical model for the interaction of transcription factors GATA-1 and PU.1. *J. Theor. Biol.* **241**, 852–865 (2006).
49. Wang J., Xu L., Wang E. & Huang S. The potential landscape of genetic circuits imposes the arrow of time in stem cell differentiation. *Biophys J.* **99**, 29–39 (2010).
50. Callura J. M., Cantor C. R. & Collins J. J. Genetic switchboard for synthetic biology applications. *Proc. Natl. Acad. Sci. USA* **109**, 5850–5855 (2012).
51. Athans M. & Falb P. L. *Optimal Control* (Dover, Mineola, NY, 2006).
52. Kurzhanski A. B. & Daryin A. N. Dynamic programming for impulse controls. *Ann. Rev. Control* **32**, 213–227 (2008).
53. Ott E. & Spano M. Controlling chaos. *Phys. Today* **48**(5), 34–40 (1995).
54. Brandt M. E. & Chen G. Bifurcation control of two nonlinear models of cardiac activity. *IEEE Trans. Circuits Syst. I, Fundam. Theory Appl.* **44**, 1031–1034 (1997).
55. Pisarchik A. N. & Goswami B. K. Annihilation of one of the coexisting attractors in a bistable system. *Phys. Rev. Lett.* **84**, 1423–1426 (2000).
56. Pisarchik A. N. Controlling the multistability of nonlinear systems with coexisting attractors. *Phys. Rev. E* **64**, 046203 (2001).
57. Bollt E. M. Targeting control of chaotic systems, in *Chaos and Bifurcations Control: Theory and Applications*, eds. Chen G., Yu X., Hill D. J. (Springer, Berlin, 2004), pp. 1–24.
58. Jackson E. A. The entrainment and migration controls of multiple-attractor systems. *Phys. Lett. A* **151**, 478–484 (1990).
59. Richter H. Controlling chaotic systems with multiple strange attractors. *Phys. Lett. A* **300**, 182–188 (2002).

60. Bazaraa M. S., Sherali H. D. & Shetty C. M. *Nonlinear Programming: Theory and Algorithms* (John Wiley & Sons Inc., Hoboken, NJ, 2006).
61. Kloeden P. E. & Platen E. *Numerical Solution of Stochastic Differential Equations* (Springer, Berlin, 1999).
62. Ott E., Sommerer J. C., Alexander J. C., Kan I. & Yorke J. A. Scaling behavior of chaotic systems with riddled basins. *Phys. Rev. Lett* **71**, 4134–4137 (1993).